OC-seislet: seislet transform construction with differential offset continuation[a]

[a]Published in Geophysics, 75, WB235-WB245, (2010)

Yang Liu[*†] *and Sergey Fomel*[†]

ABSTRACT

Many of the geophysical data analysis problems, such as signal-noise separation and data regularization, are conveniently formulated in a transform domain, where the signal appears sparse. Classic transforms such as the Fourier transform or the digital wavelet transform, fail occasionally in processing complex seismic wavefields, because of the nonstationarity of seismic data in both time and space dimensions. We present a sparse multiscale transform domain specifically tailored to seismic reflection data. The new wavelet-like transform – the *OC-seislet transform* – uses a differential offset-continuation (OC) operator that predicts prestack reflection data in offset, midpoint, and time coordinates. It provides high compression of reflection events. In the transform domain, reflection events get concentrated at small scales. Its compression properties indicate the potential of OC-seislets for applications such as seismic data regularization or noise attenuation. Results of applying the method to both synthetic and field data examples demonstrate that the OC-seislet transform can reconstruct missing seismic data and eliminate random noise even in structurally complex areas.

INTRODUCTION

Digital wavelet transforms are excellent tools for multiscale data analysis. The wavelet transform is more powerful when compared with the classic Fourier transform, because it is better fitted for representing non-stationary signals. Wavelets provide a sparse representation of piecewise regular signals, which may include transients and singularities (Mallat, 2009). In recent years, many wavelet-like transforms that explore directional characteristics of images (Starck et al., 2000; Do and Vetterli, 2005; Pennec and Mallat, 2005; Velisavljevic, 2005) were proposed. The curvelet transform in particular has found important applications in seismic imaging and data analysis (Douma and de Hoop, 2007; Chauris and Nguyen, 2008; Herrmann et al., 2008). Fomel (2006) and Fomel and Liu (2010) investigated the possibility of designing a wavelet-like transform tailored specifically to seismic data and introduced it under the name of the *seislet transform*. Based on the digital wavelet transform (DWT), the seislet transform follows patterns of seismic events (such as local slopes in 2-D and frequencies in 1-D) when analyzing those events at different scales. The seislet

transform's compression ability finds applications in common data processing tasks such as data regularization and noise attenuation. However, the problem of pattern detection limits its further applications. In 2-D, conflicting slopes at a single data point are difficult to detect reliably even using advanced methods (Fomel, 2002). It is also difficult to estimate local slopes in the presence of strong noise. A similar situation occurs in the 1-D case, in which it is difficult to exactly represent a known seismic signal using a limited set of frequencies.

Offset continuation is a process of seismic data transformation between different offsets (Deregowski and Rocca, 1981; Bolondi et al., 1982; Salvador and Savelli, 1982; Fomel, 2003c). Different types of dip moveout (DMO) operators (Hale, 1991) can be regarded as continuation to zero offset and derived as solutions to initial-value problems with the offset-continuation differential equation. In the shot-record domain, offset continuation transforms to shot continuation, which describes the process of transforming reflection seismic data along shot location (Bagaini and Spagnolini, 1996; Spagnolini and Opreni, 1996; Fomel, 2003b). The 3-D analog is known as azimuth moveout or AMO (Biondi et al., 1998; Fomel, 2003a). Bleistein and Jaramillo (2000) developed a general platform for Kirchhoff data mapping, which includes offset continuation as a special case.

In this paper, we propose to incorporate offset continuation as the prediction operator into the seislet transform. We design the transform in the log-stretch-frequency domain, where each frequency slice can be processed independently and in parallel. We expect the new seislet transform to perform better than the previously proposed seislet transform by plane-wave destruction, PWD-seislet transform (Fomel and Liu, 2010), in cases of moderate velocity variations and complex structures that generate conflicting dips in the data.

THEORETICAL BASIS

OC-seislet transform follows the same construction strategy, the lifting scheme, as the PWD-seislet transform but employs the offset-continuation operator for prediction at each transform scale.

The lifting scheme for the seislet transform

The lifting scheme (Sweldens, 1995) provides a convenient approach for designing digital wavelet transforms. The general recipe is as follows:

1. Organize the input data as a sequence of records. For OC-seislet transform of 2-D seismic reflection data, the input is in the 'frequency'-'midpoint wavenumber'-'offset' domain after the log-stretched NMO correction (Bolondi et al., 1982), and the transform direction is offset.

2. Divide the data records (along the offset axis in the case of the OC-seislet transform) into even and odd components $\mathbf{e}$ and $\mathbf{o}$. This step works at one scale level.

3. Find the residual difference $\mathbf{r}$ between the odd component and its prediction from the even component:
$$\mathbf{r} = \mathbf{o} - \mathbf{P}[\mathbf{e}] \;, \tag{1}$$
where $\mathbf{P}$ is a *prediction* operator. For example, one can obtain Cohen-Daubechies-Feauveau (CDF) 5/3 biorthogonal wavelets (Cohen et al., 1992) by defining the prediction operator as a linear interpolation between two neighboring samples,
$$\mathbf{P}[\mathbf{e}]_k = \left(\mathbf{e}_{k-1} + \mathbf{e}_k\right)/2 \;, \tag{2}$$
where k is an index number at the current scale level.

4. Find an approximation $\mathbf{c}$ of the data by updating the even component:
$$\mathbf{c} = \mathbf{e} + \mathbf{U}[\mathbf{r}] \;, \tag{3}$$
where $\mathbf{U}$ is an *update* operator. Constructing the update operator for CDF 5/3 biorthogonal wavelets aims at preserving the running average of the signal (Sweldens and Schröder, 1996):
$$\mathbf{U}[\mathbf{r}]_k = \left(\mathbf{r}_{k-1} + \mathbf{r}_k\right)/4 \;. \tag{4}$$

5. The coarse approximation $\mathbf{c}$ becomes the new data, and the sequence of steps is repeated on the new data to calculate the transform coefficients at a coarser scale level.

Next, we define new prediction and update operators using offset-continuation operators.

OC-seislet structure

We define the OC-seislet transform by specifying prediction and update operators with the help of the offset-continuation operator. Prediction and update operators for the OC-seislet transform are specified by modifying the biorthogonal wavelet construction in equations 2 and 4 as follows (Fomel, 2006; Fomel and Liu, 2010):

$$\mathbf{P}[\mathbf{e}]_k = \left(\mathbf{S}_k^{(+)}[\mathbf{e}_{k-1}] + \mathbf{S}_k^{(-)}[\mathbf{e}_k]\right)/2 \tag{5}$$
$$\mathbf{U}[\mathbf{r}]_k = \left(\mathbf{S}_k^{(+)}[\mathbf{r}_{k-1}] + \mathbf{S}_k^{(-)}[\mathbf{r}_k]\right)/4 \;, \tag{6}$$

where $\mathbf{S}_k^{(+)}$ and $\mathbf{S}_k^{(-)}$ are operators that predict the data record (a common-offset section) by differential offset continuation from its left and right neighboring common-offset sections with different offsets. Offset continuation operators provide the physical

connection between data records. The theory of offset continuation is reviewed in Appendix A.

One can also employ a higher-order transform, for example, by using the template of the CDF 9/7 biorthogonal wavelet transform, which is used in JPEG-2000 compression (Lian et al., 2001). There is only one stage (one prediction and one update) for the CDF 5/3 wavelet transform, but there are two cascaded stages and one scaling operation for CDF 9/7 wavelet transform. Prediction and update operators for a high-order OC-seislet transform are defined as follows:

$$\mathbf{P}_1[\mathbf{e}]_k = (\mathbf{S}_k^{(+)}[\mathbf{e}_{k-1}] + \mathbf{S}_k^{(-)}[\mathbf{e}_k]) \cdot \alpha \ , \tag{7}$$

$$\mathbf{U}_1[\mathbf{r}]_k = (\mathbf{S}_k^{(+)}[\mathbf{r}_{k-1}] + \mathbf{S}_k^{(-)}[\mathbf{r}_k]) \cdot \beta \ , \tag{8}$$

$$\mathbf{P}_2[\mathbf{e}]_k = (\mathbf{S}_k^{(+)}[\mathbf{e}_{k-1}] + \mathbf{S}_k^{(-)}[\mathbf{e}_k]) \cdot \gamma \ , \tag{9}$$

$$\mathbf{U}_2[\mathbf{r}]_k = (\mathbf{S}_k^{(+)}[\mathbf{r}_{k-1}] + \mathbf{S}_k^{(-)}[\mathbf{r}_k]) \cdot \delta \ , \tag{10}$$

where the subscripts 1 and 2 represent the first and the second stage. α, β, γ, and δ are defined numerically as follows:

$$\begin{aligned} \alpha &= -1.586134342, \\ \beta &= -0.052980118, \\ \gamma &= 0.882911076, \\ \delta &= 0.443506852. \end{aligned}$$

One can combine equations 1, 3, 7, and 8 to finish the first stage, and repeatedly process the result by using equations 1, 3, 9, and 10. The scale normalization factors correspond to the CDF 9/7 biorthogonal wavelet transform (Daubechies and Sweldens, 1998). Scaling and coefficients are as follows:

$$\mathbf{e} = \mathbf{e} \cdot K \ , \tag{11}$$

$$\mathbf{o} = \mathbf{o} \cdot (1/K) \ , \tag{12}$$

where K= 1.230174105.

We used the high-order version of OC-seislet transform to process the synthetic and field data examples used in this paper.

Simple example

Figure 1 shows a 2-D slice out of the benchmark French model (French, 1974). We created a 2-D prestack dataset (Figure 2a) by Kirchhoff modeling. Three sections in Figure 2a show the time slice at time position 0.6 s (top section), common-offset section at offset position of 0.2 km (bottom-left section), and common-midpoint gather at midpoint position of 1.0 km (bottom-right section). The reflector with a round

dome and corners creates complicated reflection events along both midpoint and offset axes. The inflection points of the reflector leads to traveltime triplications at some offsets. Figure 2b shows a preprocessed data cube in the F-K-offset domain after the log-stretched NMO correction and a double Fourier transform along the stretched time and midpoint axes. We apply the OC-seislet transform described above along the offset axis in Figure 2b. Thus, the offset axis becomes the scale axis. The cube of the transform coefficients is shown in Figure 3b and should be compared with the corresponding Fourier transform along the offset direction in Figure 3a. The OC-seislet transform coefficients get concentrated at small scales, which enables an effective compression. In contrast, the Fourier transform develops large coefficients at coarser scales but has small residual coefficients at fine scales. Figure 4 shows a comparison between the decay of coefficients (sorted from large to small) between the Fourier transform and the OC-seislet transform. A significantly faster decay of the OC-seislet coefficients is evident.

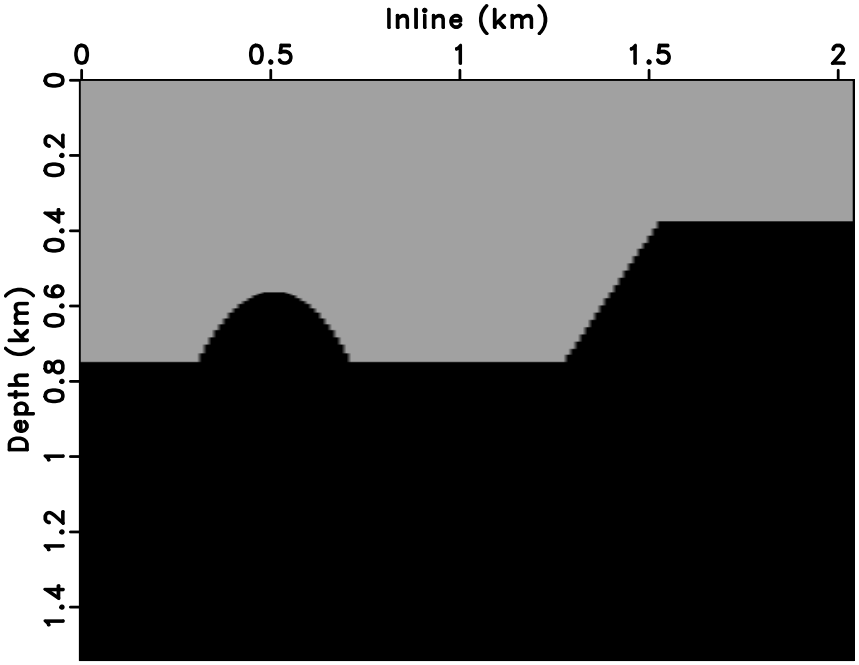

Figure 1: 2-D slice out of the benchmark French model (French, 1974).

Iterative soft-thresholding

The proposed OC-seislet transform uses physical offset continuation to compress the reflection data after NMO and log-stretch transform of the time coordinate, followed by double Fourier transforms of the stretched time axis and midpoint axis. If seismic traces in the midpoint direction are missing, the Fourier transform may produce artifacts (spatial leakage) along the midpoint-wavenumber axis (Zwartjes and Gisolf, 2007). Additionally, the missing seismic traces in the offset direction affect the conti-

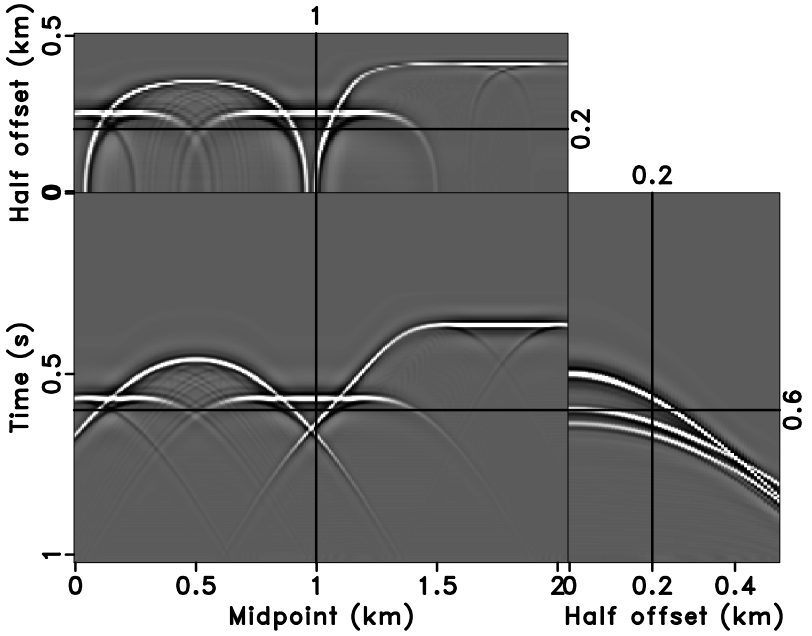

(a)

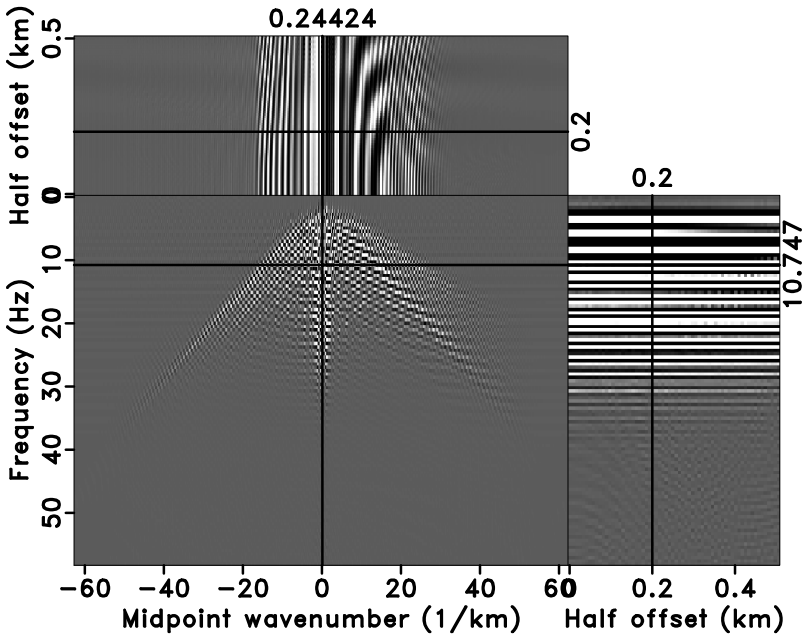

(b)

Figure 2: 2-D synthetic prestack data in t-x-offset domain (a) and in F-K-offset domain (b).

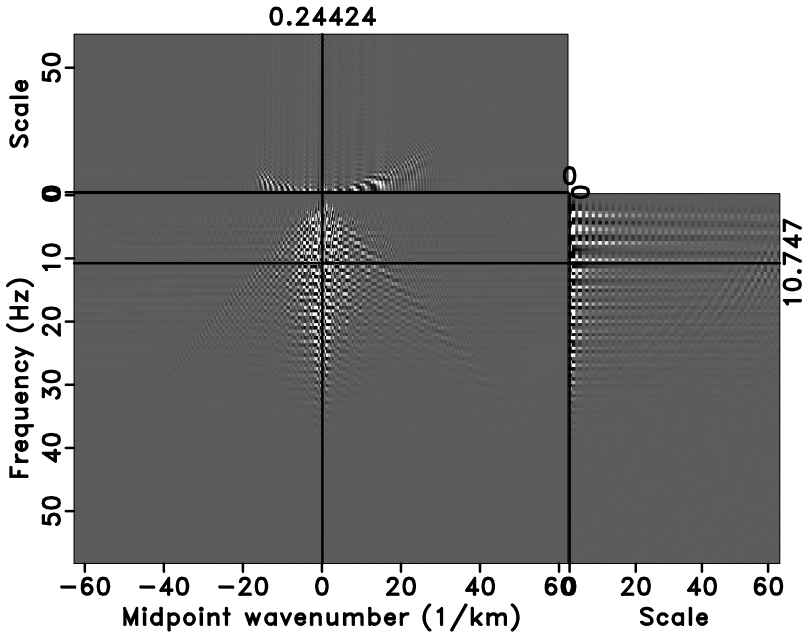

(a)

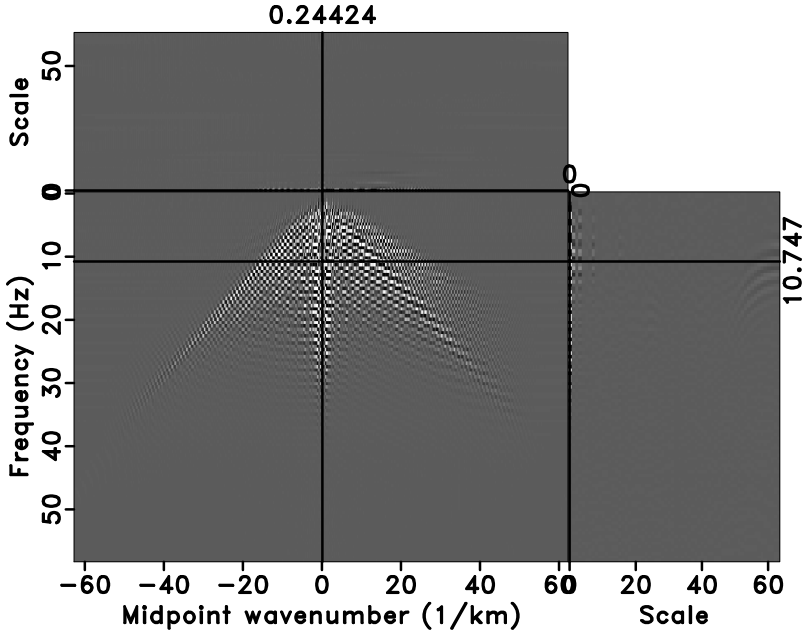

(b)

Figure 3: Fourier transform (a) and OC-seislet transform (b) of the input data from Figure 2b along the offset axis.

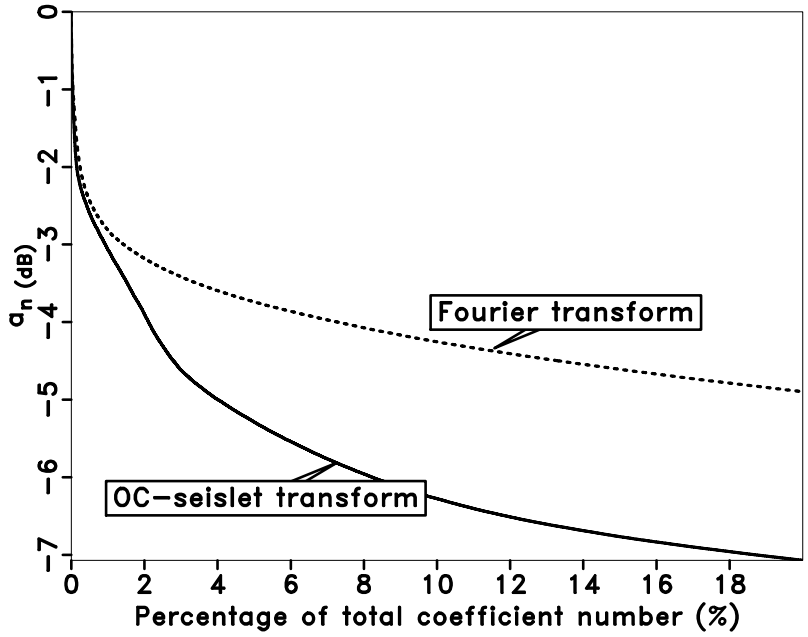

Figure 4: Transform coefficients sorted from large to small, normalized, and plotted on a decibel scale. Solid line: OC-seislet transform. Dashed line: Fourier transform.

nuity of predicted data. Once the OC-seislet transform is applied for predicting and compressing, the artifacts, discontinuity information, and random noise spread over different scales while the predictable reflection information gets compressed to large coefficients at small scales. A simple thresholding method can easily remove the small coefficients of artifacts. Finally, applying inverse OC-seislet transform, inverse FFTs both in time and midpoint axes, inverse log-stretch, and inverse NMO reconstructs the data while attenuating random noise, reducing artifacts along the midpoint axis, reconstructing continuity in the offset axis, and recovering main structural features without using any assumptions about structural continuity in the midpoint-offset-time domain. The key steps are shown in Figure 5a.

The idea of sparse transforms has been thoroughly explored in the literature, with application to Fourier and curvelet transforms. Liu and Sacchi (2004) proposed a Fourier-based minimum weighted norm interpolation (MWNI) algorithm with iterative inversion to perform multidimensional reconstruction of seismic wavefields. Xu et al. (2005) suggested an iterative Fourier-based matching pursuit (antileakage Fourier transform) for seismic data regularization. Abma and Kabir (2006) used a Fourier-based method with iterative thresholding to solve seismic data interpolation problems. Herrmann and Hennenfent (2008) presented a recovery method that exploits the curvelet frame. Missing data interpolation is a particular case of data regularization, where the input data are already given on a regular grid, and one needs to reconstruct only the missing values in empty bins (Fomel, 2001). For input data with nonuniform spatial sampling, one can bin the data to a regular grid first and then use the proposed method for filling empty bins. It is also possible to

generalize the method for combining irregular data interpolation with a sparse transform (Zwartjes and Gisolf, 2007). The thresholding iteration helps a sparse transform to recover the missing information. We adopt a similar thresholding strategy (fixed thresholding value for each iteration) with the OC-seislet transform. The key steps of the algorithm are illustrated schematically in Figure 5b.

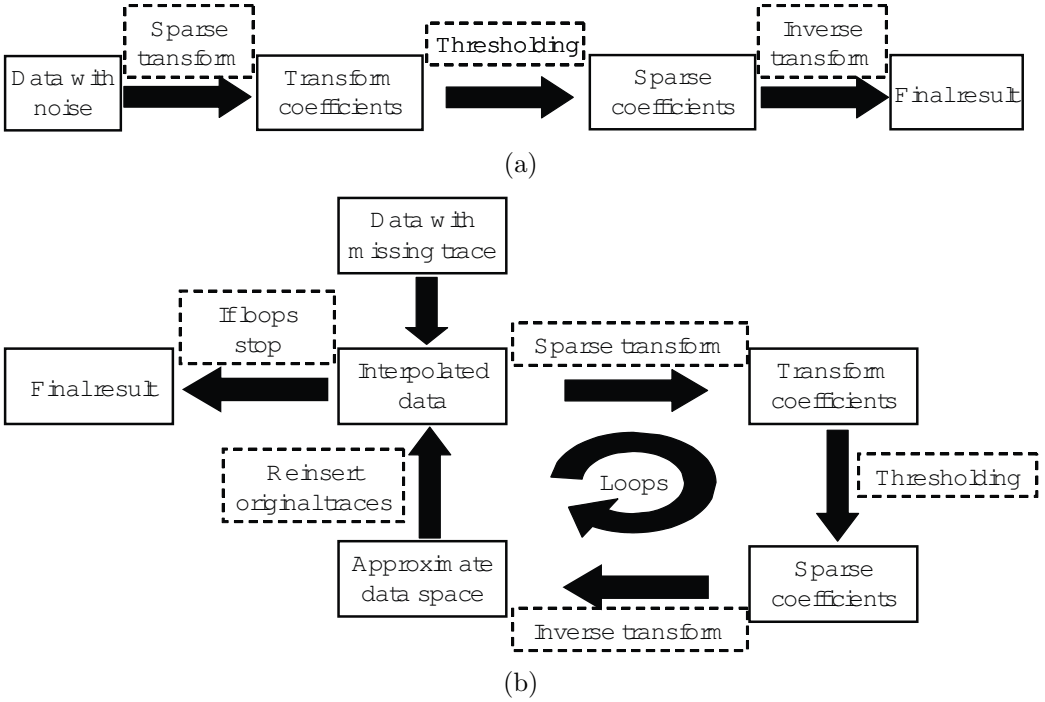

Figure 5: Schematic illustration of the thresholding workflow. Denoising with a simple soft-thresholding (a) and missing data interpolation with iterative soft-thresholding (b).

SYNTHETIC DATA TESTS

We continue to use the synthetic model from Figure 1 to test the proposed method. Figure 6 is the data with normally-distributed random noise added. Figure 7a shows the datacube in the F-K-offset domain after the log-stretched NMO correction and a double Fourier transform along the stretched time axis and midpoint axis. We run the OC-seislet transform in parallel on individual frequency slices. Figure 7b shows the OC-seislet coefficients. All reflection information is concentrated in a small scale range. However, since random noise cannot be predicted well by the offset-continuation operator, it spreads throughout the whole transform domain. The inverse Fourier transform both in time and midpoint directions and the inverse log-stretch return the OC-seislet coefficients to the time-midpoint-scale domain. The coefficients at the zero scale represent stacking along the offset direction, which is equivalent to the DMO stack (Figure 8b).

We use a soft-thresholding method to separate reflection and random noise in the OC-seislet domain. Figure 8a displays the result after the inverse OC-seislet transform. Compared with Figure 7a, data in the F-K-offset domain contain only useful information. Figure 9b shows the denoising result in the t-x-offset domain after the double inverse Fourier transform, the inverse log-stretch and the inverse NMO. All characteristics of reflection and diffraction events are preserved well. For comparison, we used PWD-seislet transform and soft-thresholding method with the same threshold values to process the noisy data (Figure 6). The result is shown in Figure 9a. Because PWD-seislet transform is based on the local dip information, a mixture of different dips from the triplications makes it difficult to process the data in individual common-midpoint gathers. The PWD-seislet transform compresses all information along the local events slopes in each common-midpoint gather. It separates reflection signal and noise but smears the crossing events, especially at the far offset. The corresponding signal-to-noise ratios for denoised results with PWD-seislet transform and OC-seislet transform are 24.95 dB and 41.45 dB, respectively. The differences (Figure 10) between noisy data (Figure 6) and denoised results with PWD-seislet transform (Figure 9a) and OC-seislet transform (Figure 9b) further illustrate the effectiveness of the OC-seislet transform.

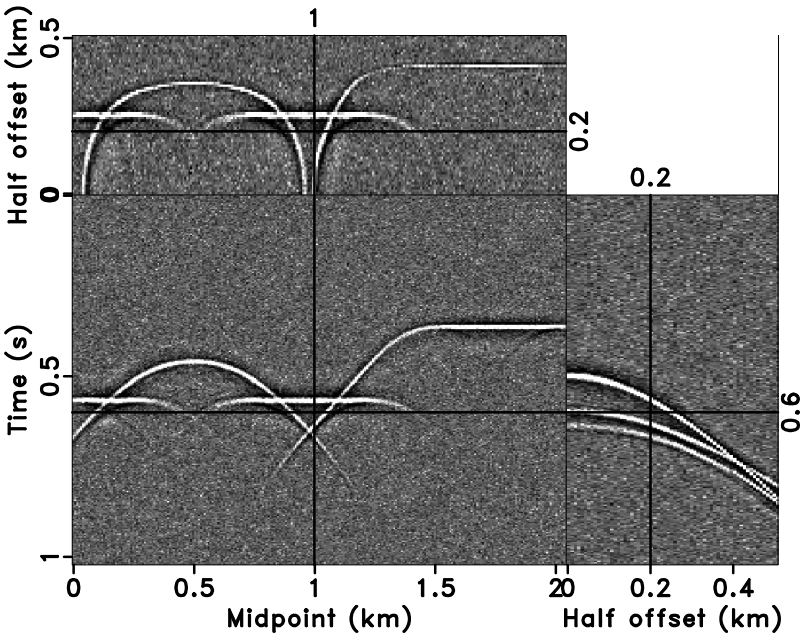

Figure 6: 2-D noisy data in t-x-offset domain.

For a data regularization test, we remove 80% of randomly selected traces (Figure 11a) from the ideal data (Figures 2a). The complex dip information makes it extremely difficult to interpolate the data in individual common-offset gathers. The dataset is also non-stationary in the offset direction. Therefore, a simple offset interpolation scheme would also fail. Figure 11b shows the data after NMO correction, log-stretch transform, and double Fourier transforms. The missing traces introduce spatial artifacts in midpoint-wavenumber axis and discontinuities along the offset di-

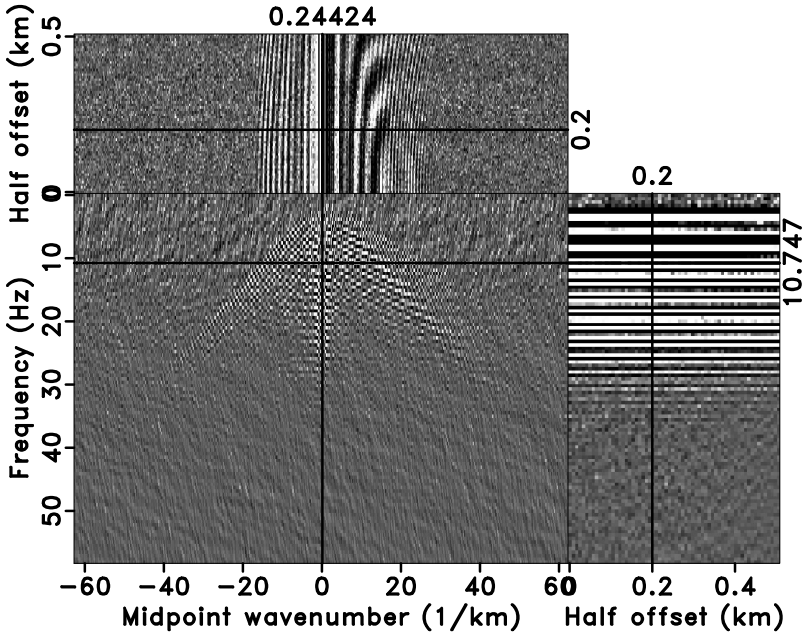

(a)

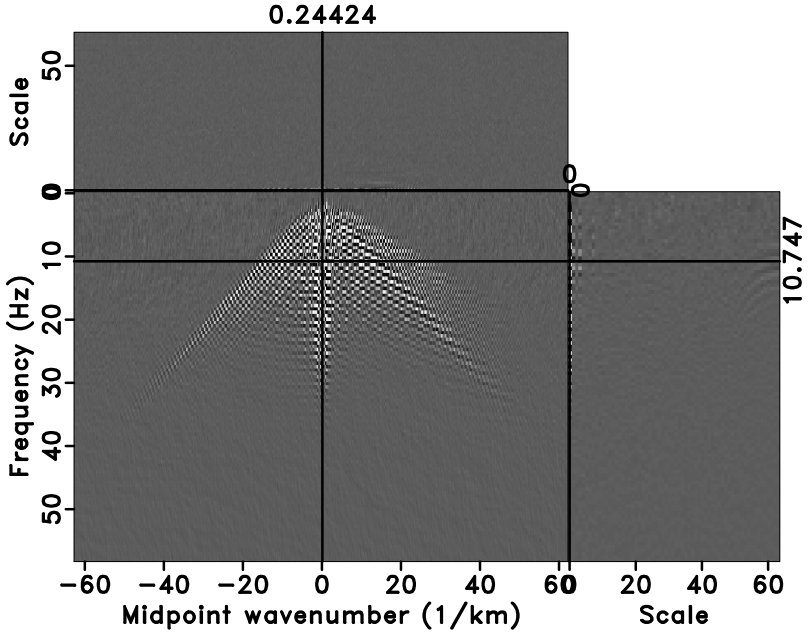

(b)

Figure 7: Noisy data in F-K-offset domain (a) and OC-seislet coefficients in F-K-scale domain (b).

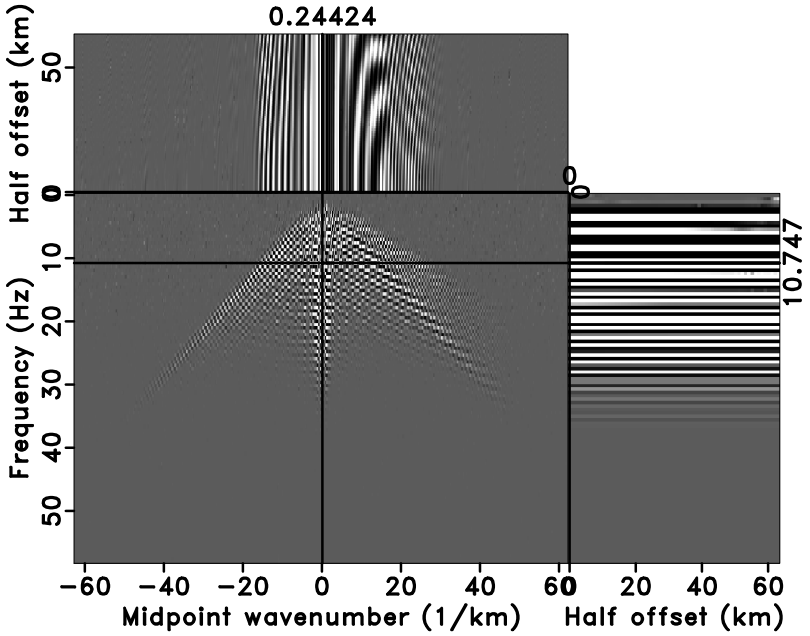

(a)

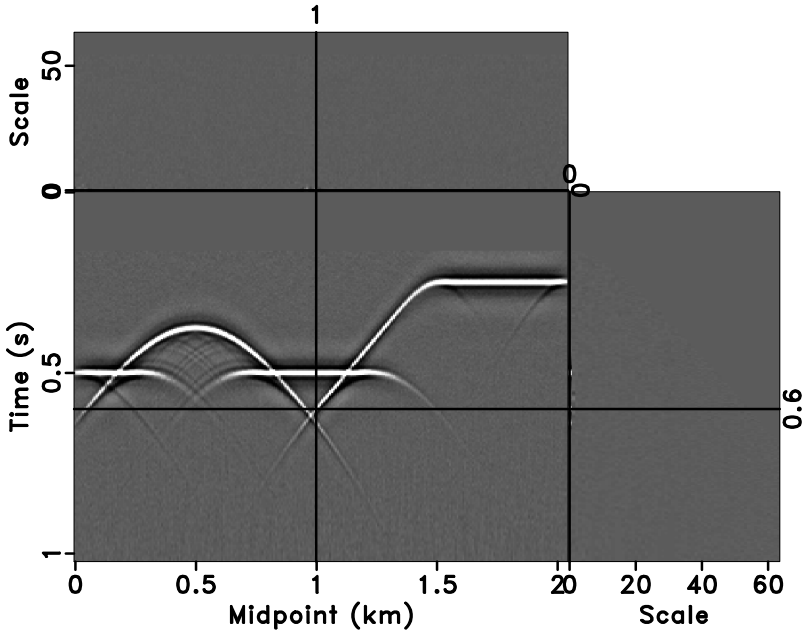

(b)

Figure 8: Thresholded data in F-K-offset domain (a) and OC-seislet coefficients in t-x-scale domain (b).

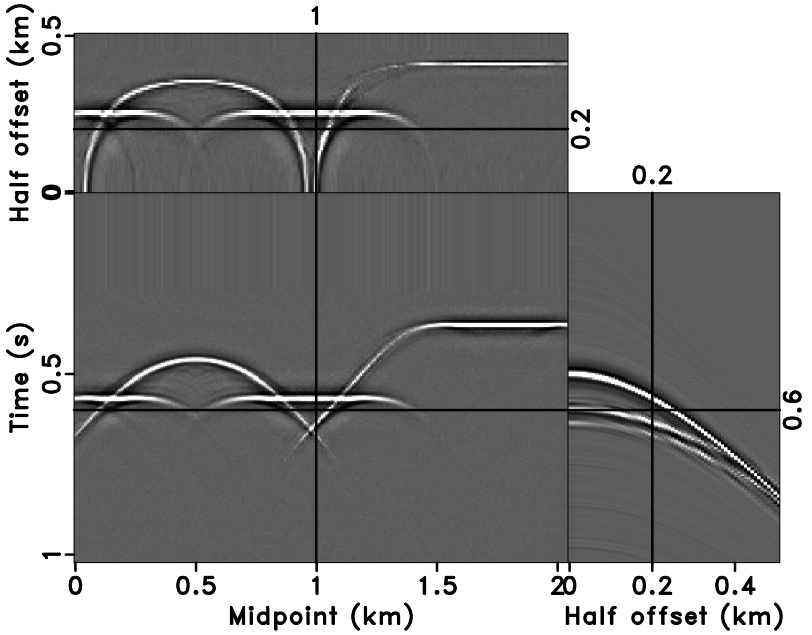

(a)

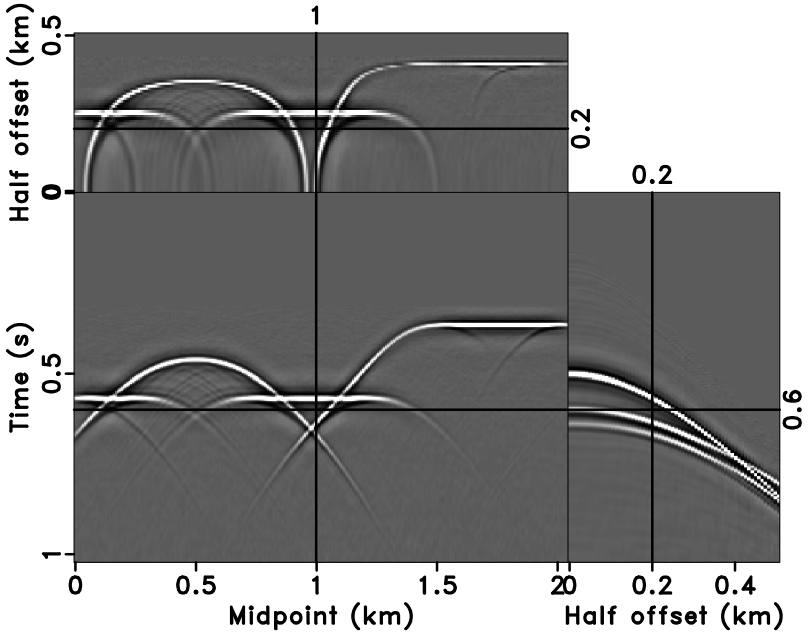

(b)

Figure 9: Denoised result by different methods. PWD-seislet transform (a) and OC-seislet transform (b). (Compare with Figure 2.)

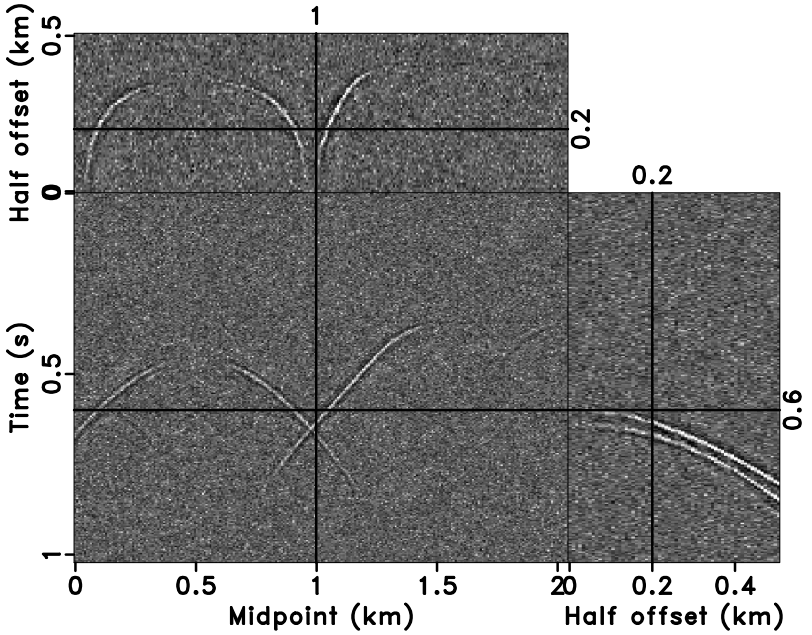

(a)

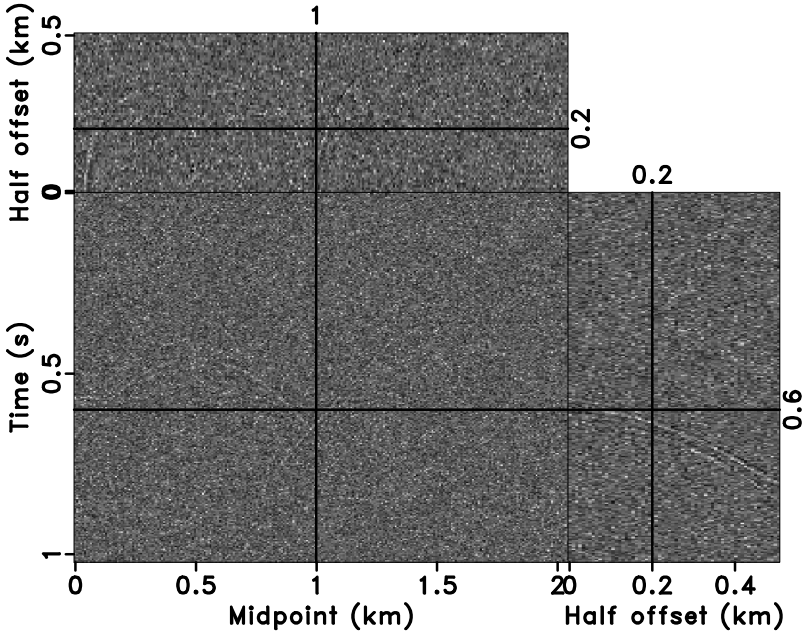

(b)

Figure 10: Difference between noisy data (Figure 6) and denoised results with different methods (Figure 9). PWD-seislet transform (a) and OC-seislet transform (b).

rection. After the OC-seislet transform, the reflection information can be predicted and compressed. Meanwhile, the artifacts spread over the whole transform domain (Figure 12a). The simple soft-thresholding algorithm (i.e., the iterative strategy with only one iteration) removes most of the artifacts, and the inverse OC-seislet transform reconstructs the major reflection information according to the offset-continuation prediction (Figure 12b).

One can also employ an iterative soft-thresholding strategy to implement missing data interpolation. This method recovers missing traces as long as seismic data are sparse enough in the transform domain. To demonstrate the superior sparseness of the OC-seislet coefficients, we compare the proposed method with the 3-D Fourier transform. Figure 13a displays the interpolated result after a 3-D Fourier interpolation using iterative thresholding (Abma and Kabir, 2006). The Fourier transform cannot provide enough sparseness of coefficients for complex reflections and, therefore, fails in recovering all missing traces. The OC-seislet transform is based on a physical prediction, and provides a much sparser domain for both reflections and diffractions. Iterative thresholding succeeds in interpolating the missing traces (Figure 13b).

FIELD DATA TESTS

We use a historic marine dataset from the Gulf of Mexico (Claerbout, 2000) to evaluate the proposed method for both noise attenuation and missing data interpolation problems. The input data are shown in Figure 14a. Near- and far- offset information is completely missing. After log-stretched NMO and Fourier transforms along time and midpoint axes convert the original data from time-midpoint-offset domain to frequency-wavenumber-offset domain, the OC-seislet transform compresses the predictable information according to the physical connection between different offsets. Unpredictable artifacts and reflections display different tendencies: artifacts disperse throughout the whole transform domain while reflections are compressed to a small scale range (Figure 14b). If we choose the significant coefficients using soft-thresholding, the inverse processing steps (including the inverse OC-seislet transform, the inverse FFTs both in time and midpoint axes, and the inverse log-stretch NMO) effectively remove incoherent artifacts from the data (Figure 15a). The difference between input data (Figure 14a) and denoised result (Figure 15a) is shown in Figure 15b. Most coherent events including reflections and diffractions are well protected by the proposed method thanks to the ability of the offset-continuation operator to predict structurally complex wavefields. However, some energy of the events is partly missing. To achieve a better result, one may need to use a more accurate NMO velocity. Thus, denoising is a naturally defined operation in the OC-seislet domain. The soft-thresholding techniques eliminate only part of spatial aliasing because of sparse offset sampling. Additional offset interpolation can further remove spatial aliasing.

For a data regularization test, we removed 70% of randomly selected traces from the input data (Figure 16). After applying the OC-seislet transform and iterative soft-thresholding, spatial artifacts and offset discontinuity in the transform domain coming

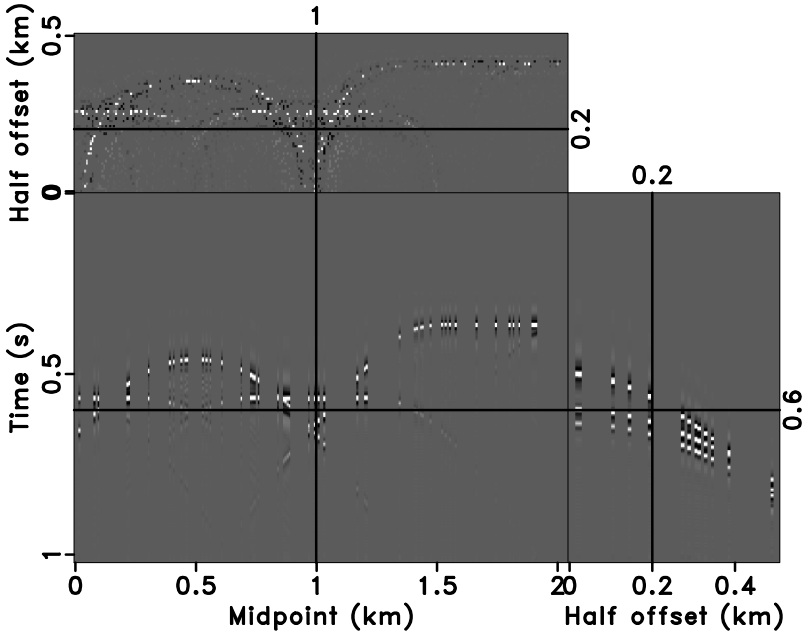

(a)

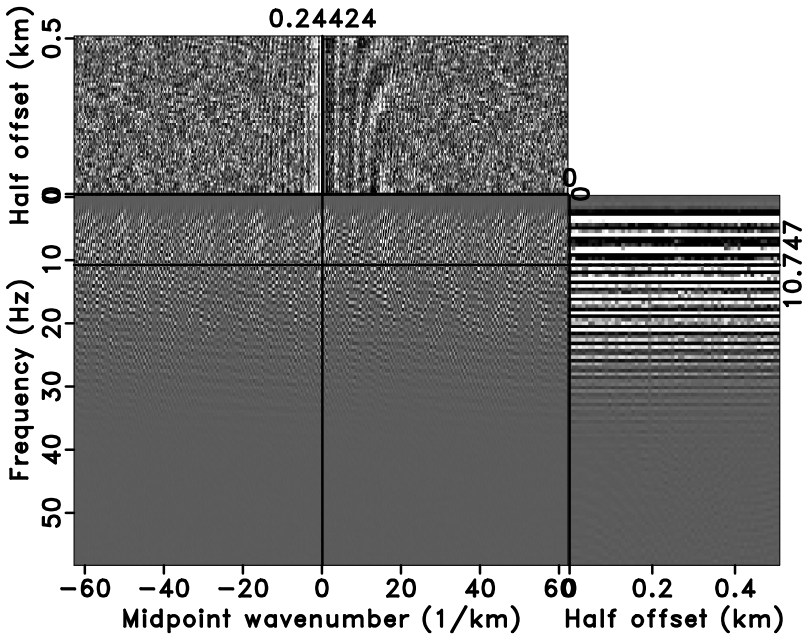

(b)

Figure 11: Synthetic data with 80% traces removed (a) and missing data in F-K-offset domain (b).

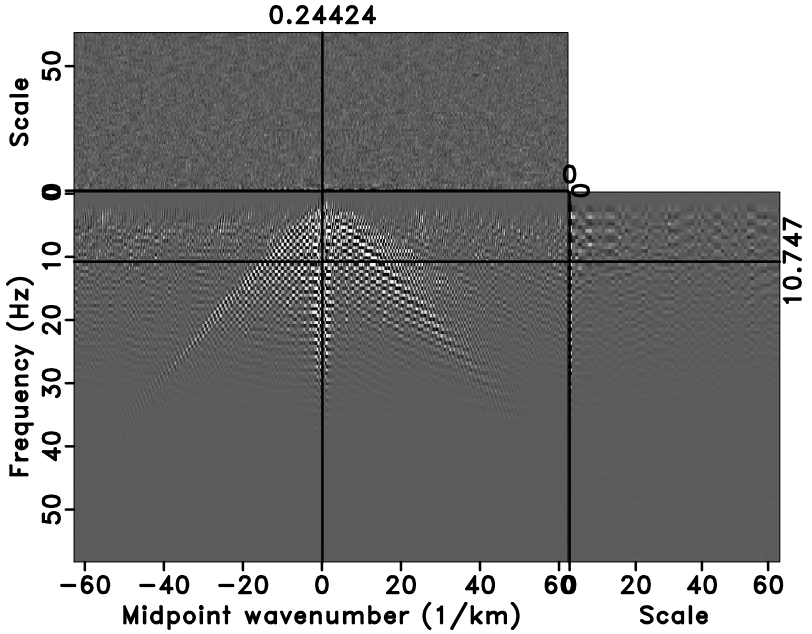

(a)

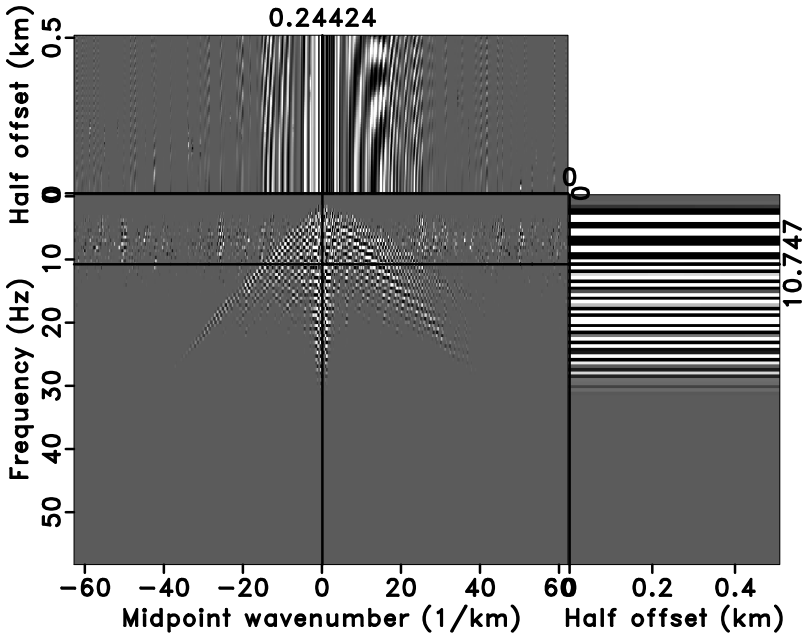

(b)

Figure 12: OC-seislet coefficients in F-K-scale domain (a) and data of iteration 1 after soft-thresholding in F-K-offset domain (b).

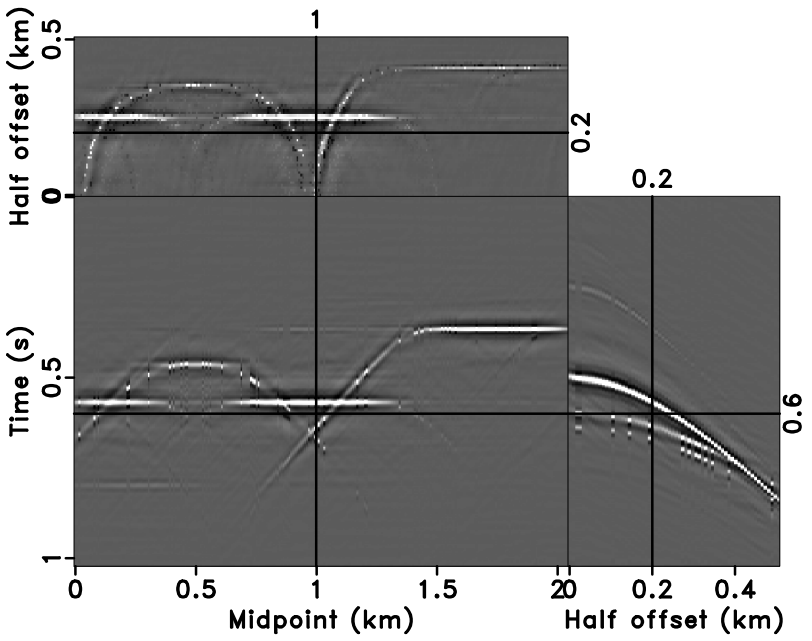

(a)

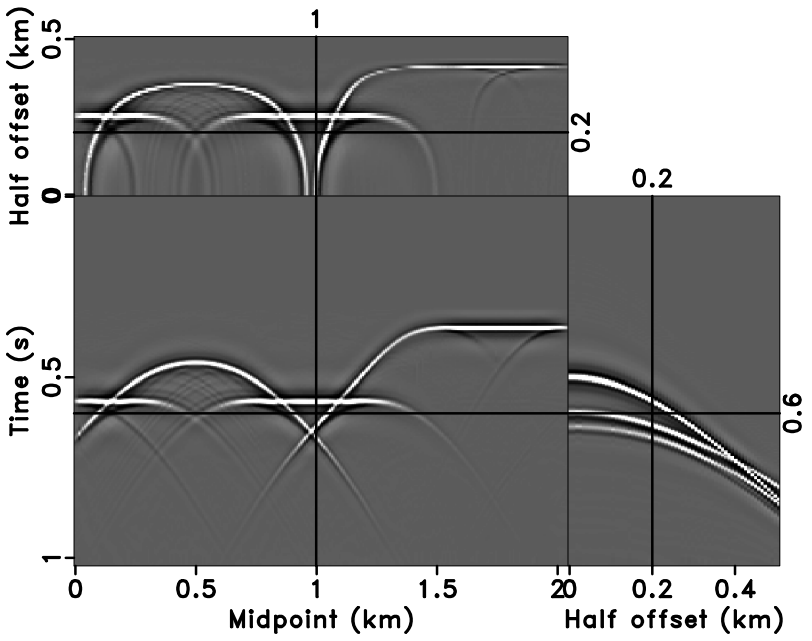

(b)

Figure 13: Interpolated results using iterative thresholding with different sparse transforms. 3-D Fourier transform (a) and OC-seislet transform (b). (Compare with Figure 2)

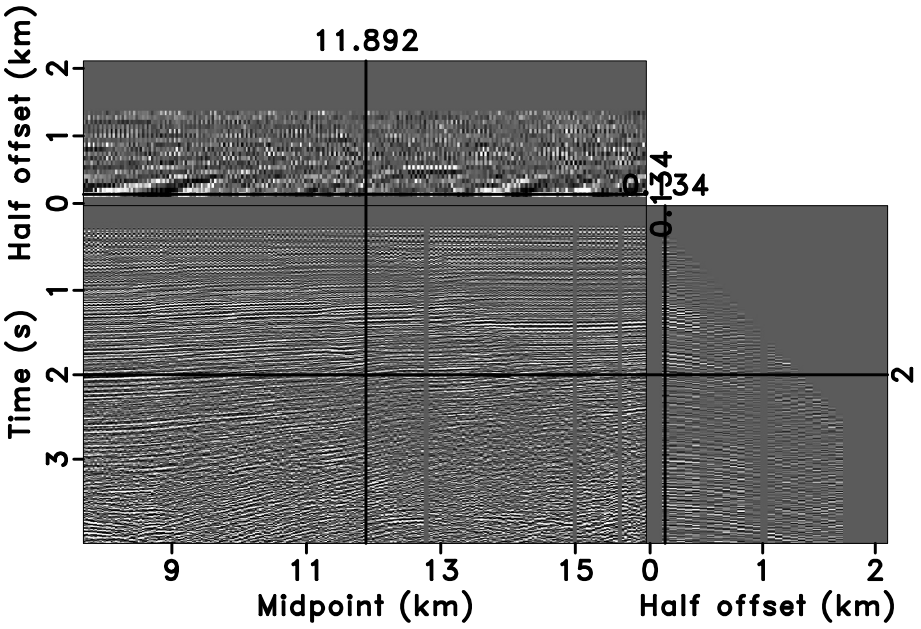

(a)

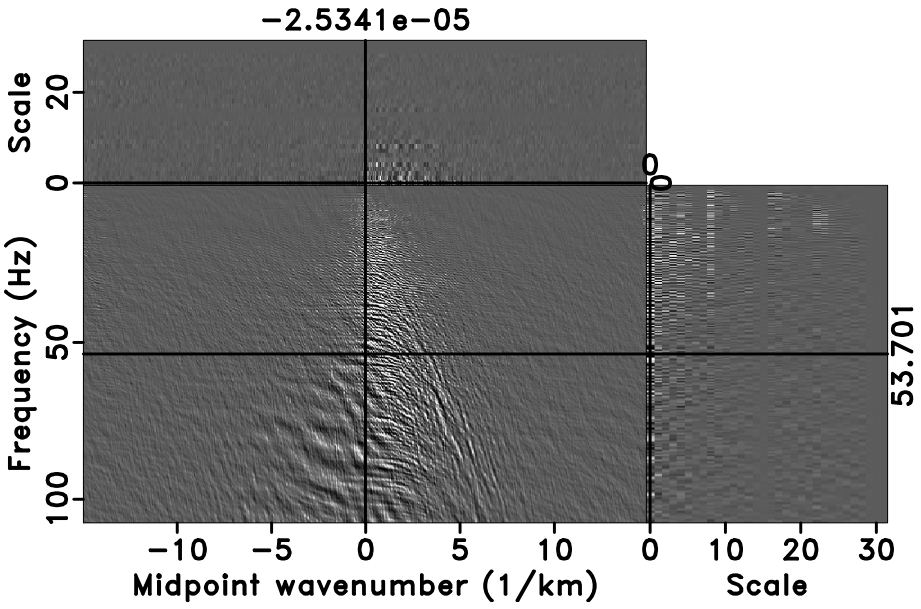

(b)

Figure 14: Marine data in t-x-offset domain (a) and OC-seislet coefficients in F-K-scale domain (b).

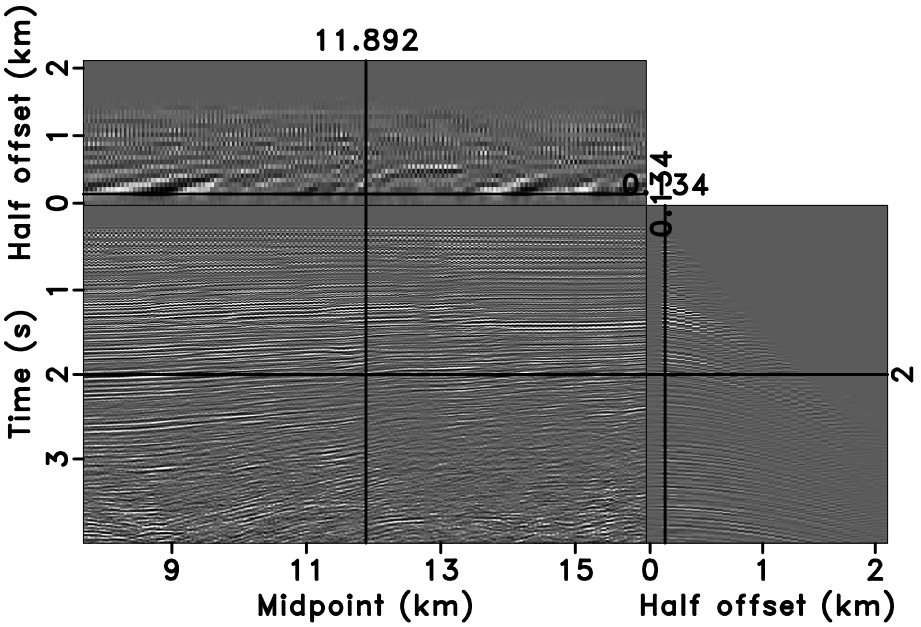

(a)

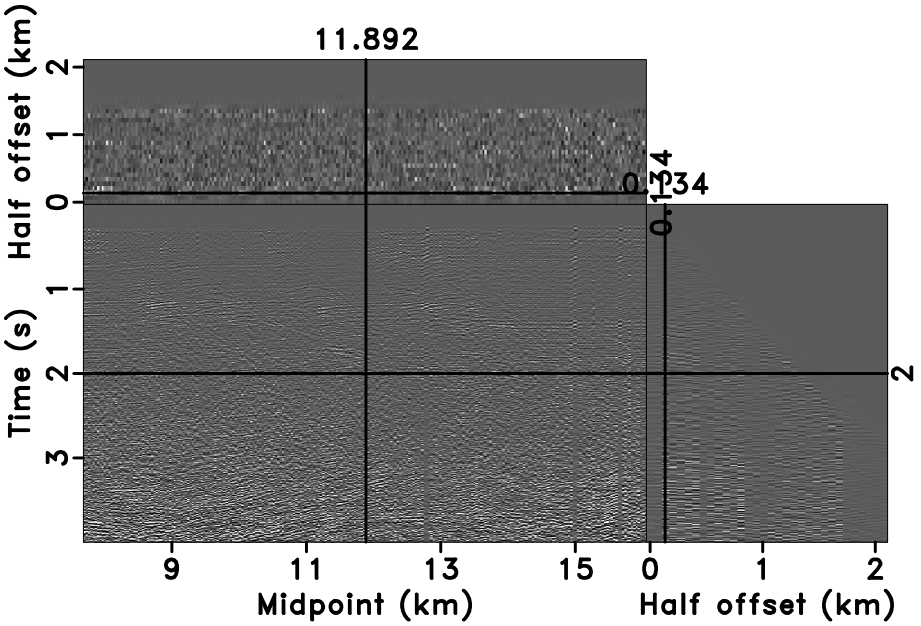

(b)

Figure 15: Denoised result in t-x-offset domain (a) and difference between input data (Figure 14a) and denoised result (Figure 15a) (b).

from missing traces get attenuated. The interpolated result is shown in Figure 17b. Missing traces have been interpolated well even where diffractions are present. For comparison, we applied 3-D Fourier transform with iterative soft-thresholding, as proposed by Abma and Kabir (2006). The same parameters of soft-thresholding for those in the OC-seislet transform were used. The final result is shown in Figure 17a. The Fourier transform fails to recover the missing information as accurately as the OC-seislet transform. Fundamentally, the Fourier coefficients are simply not sparse enough for this dataset. Figure 18 shows the comparison after DMO stacking. The result from 3-D Fourier transform displays obvious gaps which are caused by inperfect interpolation (Figure 18a), while the OC-seislet transform and iterative soft-thresholding strategy provide a reasonably accurate result (Figure 18b).

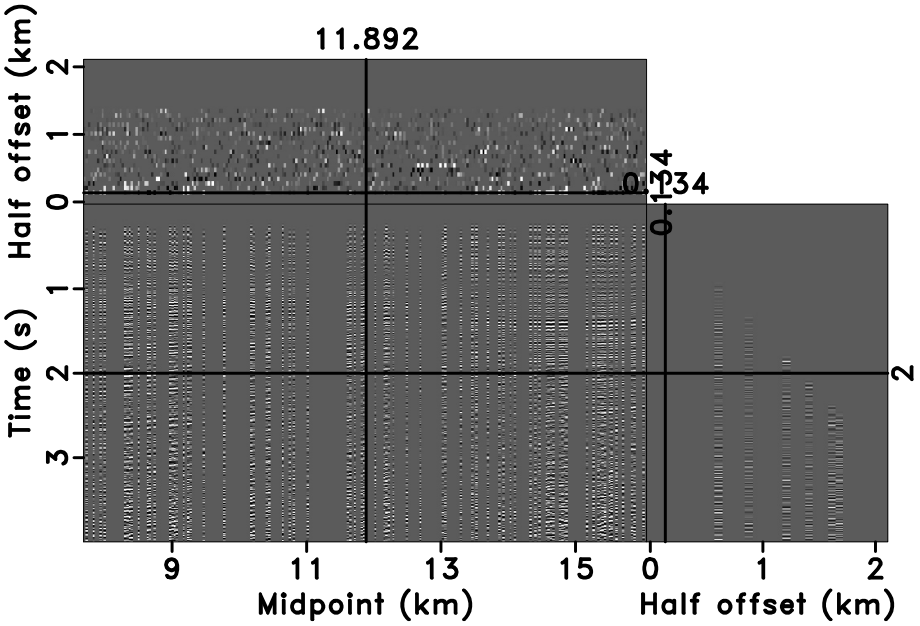

Figure 16: Marine data with 70% traces removed.

CONCLUSIONS

We have introduced the OC-seislet transform, a new domain for analyzing prestack reflection data in offset, midpoint, and time coordinates. Thanks to its physical basis, the new transform is able to characterize and compress structurally complex seismic data better than either the 3-D Fourier transform or the PWD-seislet transform. The offset-continuation operator serves as a transformational bridge between different offsets, which allows the OC-seislet transform to compress all predictable reflections and diffractions into small scales. In the new transform domain, random noise spreads over different scales while the predictable reflection seismic events get compressed to large coefficients at small scales. Therefore, a thresholding approach is successful in separating seismic signal and noise. Reconstructing missing seismic data is a more

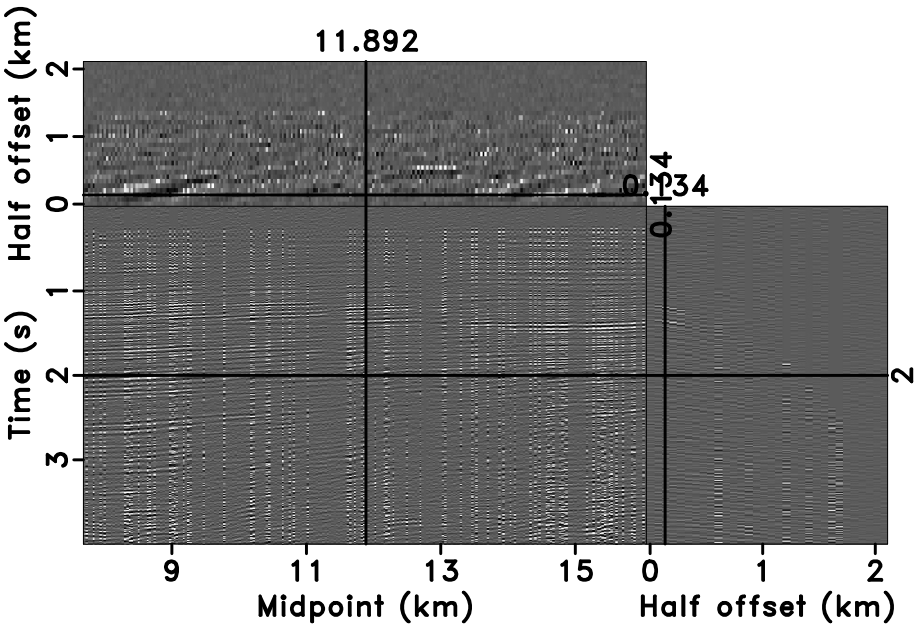

(a)

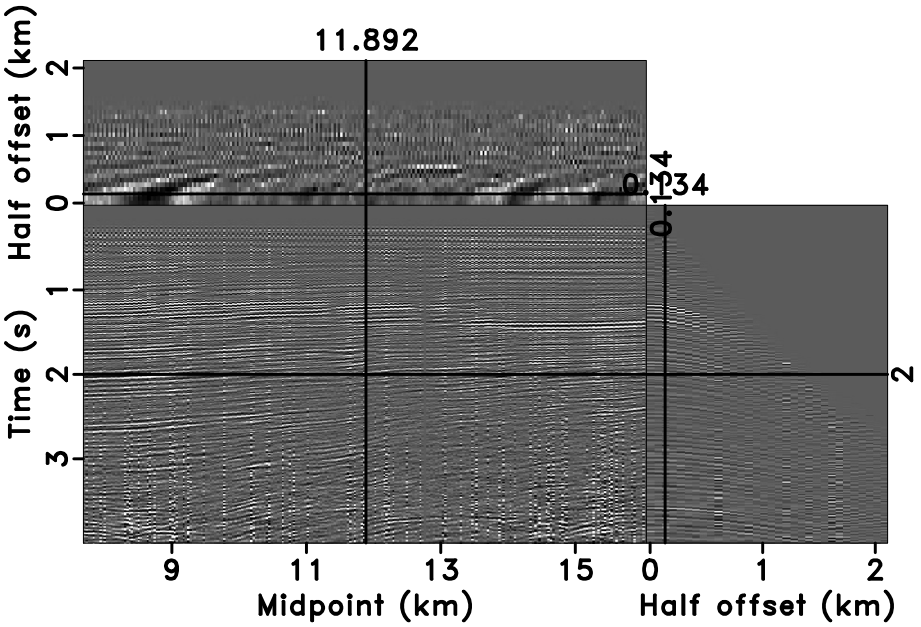

(b)

Figure 17: Interpolated results using iterative thresholding with different transforms. 3-D Fourier transform (a) and OC-seislet transform (b).

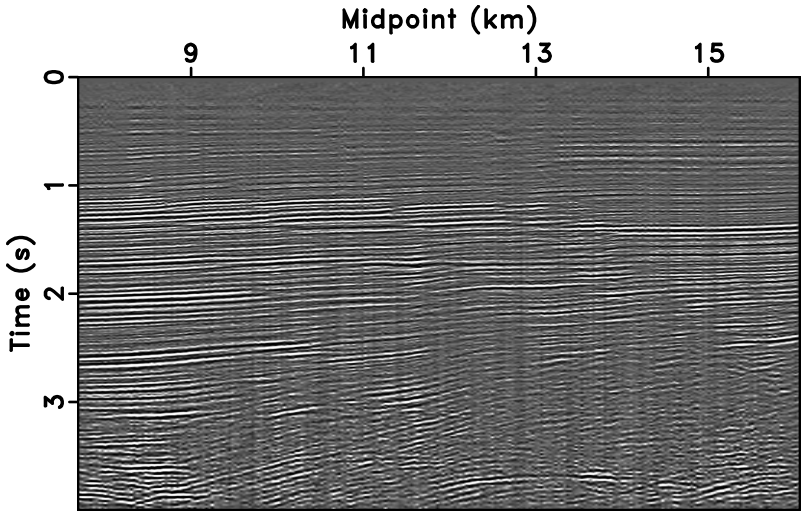

(a)

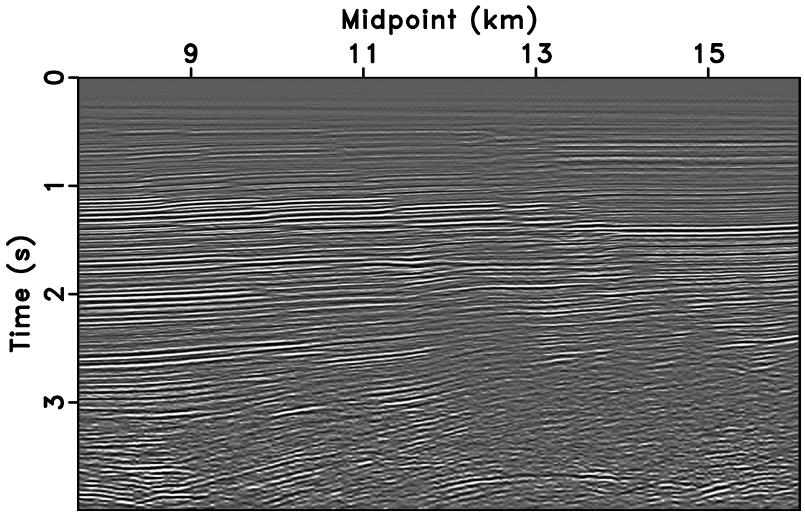

(b)

Figure 18: Stacking of interpolated results corresponding to Figure 17. 3-D Fourier transform (a) and OC-seislet transform (b).

difficult task, where iterative thresholding is required to help the proposed OC-seislet transform recover the missing seismic traces. Tests using both synthetic and field data demonstrate that the proposed transform can succeed in handling structurally complex data even in the presence of strong random noise.

ACKNOWLEDGMENTS

We thank BGP Americas for a partial financial support of this work. We thank Tamas Nemeth, Mauricio Sacchi, Sandra Tegtmeier-Last, and two anonymous reviewers for their constructive comments and suggestions. This publication was authorized by the Director, Bureau of Economic Geology, The University of Texas at Austin.

APPENDIX A

REVIEW OF DIFFERENTIAL OFFSET CONTINUATION

In this appendix, we review the theory of differential offset continuation from Fomel (2003a,c). The partial differential equation for offset continuation (differential azimuth moveout) takes the form

$$\left(\mathbf{h}^T \mathbf{P}_{xx}\, \mathbf{h} - h^2\, \frac{\partial^2 P}{\partial h^2}\right) \;=\; h\, t_n\, \frac{\partial^2 P}{\partial t_n\, \partial h}\;, \tag{A-1}$$

where $P(\mathbf{x}, \mathbf{h}, t_n)$ is the seismic data in the midpoint-offset-time domain, t_n is the time coordinate after the normal moveout (NMO) correction, $\mathbf{h}^T$ denotes the transpose of $\mathbf{h}$, and $\mathbf{P}_{xx}$ is the tensor of the second-order midpoint derivatives.

A particularly efficient implementation of offset continuation results from a log-stretch transform of the time coordinate (Bolondi et al., 1982), followed by a Fourier transform of the stretched time axis. After these transforms, the offset-continuation equation takes the form

$$\left(\mathbf{h}^T \tilde{\mathbf{P}}_{xx}\, \mathbf{h} - h^2\, \frac{\partial^2 \tilde{P}}{\partial h^2}\right) \;=\; i\,\Omega\, h\, \frac{\partial \tilde{P}}{\partial h}\;, \tag{A-2}$$

where Ω is the dimensionless frequency corresponding to the stretched time coordinate and $\tilde{P}(\mathbf{x}, \mathbf{h}, \Omega)$ is the transformed data. As in other frequency-space methods, equation A-2 can be applied independently and in parallel on different frequency slices.

In the frequency-wavenumber domain, the extrapolation operator is defined by solving an initial-value problem for equation A-2. The analytical solution takes the form

$$\tilde{\tilde{P}}(\mathbf{k}, \mathbf{h}_2, \Omega) = \tilde{\tilde{P}}(\mathbf{k}, \mathbf{h}_1, \Omega)\, \frac{Z_\lambda(\mathbf{k}\cdot\mathbf{h}_2)}{Z_\lambda(\mathbf{k}\cdot\mathbf{h}_1)}\;, \tag{A-3}$$

where $\tilde{\tilde{P}}(\mathbf{k},\mathbf{h},\Omega)$ is the double-Fourier-transformed data, $\lambda=(1+i\Omega)/2$, Z_λ is the special function defined as

$$Z_\lambda(x)=\Gamma(1-\lambda)\left(\frac{x}{2}\right)^\lambda J_{-\lambda}(x)={}_0F_1\left(;1-\lambda;-\frac{x^2}{4}\right)\ , \tag{A-4}$$

Γ is the gamma function, $J_{-\lambda}$ is the Bessel function, and ${}_0F_1$ is the confluent hypergeometric limit function (Petkovsek et al., 1996). The wavenumber $\mathbf{k}$ in equation A-3 corresponds to the midpoint $\mathbf{x}$ in the original data domain. In high-frequency asymptotics, the offset-continuation operator takes the form

$$\tilde{\tilde{P}}(\mathbf{k},\mathbf{h}_2,\Omega)\approx\tilde{\tilde{P}}(\mathbf{k},\mathbf{h}_1,\Omega)\,\frac{F(\frac{2\mathbf{k}\cdot\mathbf{h}_2}{\Omega})\,\exp\left[i\Omega\,\psi\left(\frac{2\mathbf{k}\cdot\mathbf{h}_2}{\Omega}\right)\right]}{F(\frac{2\mathbf{k}\cdot\mathbf{h}_1}{\Omega})\,\exp\left[i\Omega\,\psi\left(\frac{2\mathbf{k}\cdot\mathbf{h}_1}{\Omega}\right)\right]}\ , \tag{A-5}$$

where

$$F(\epsilon)=\sqrt{\frac{1+\sqrt{1+\epsilon^2}}{2\sqrt{1+\epsilon^2}}}\,\exp\left(\frac{1-\sqrt{1+\epsilon^2}}{2}\right)\ , \tag{A-6}$$

and

$$\psi(\epsilon)=\frac{1}{2}\left(1-\sqrt{1+\epsilon^2}+\ln\left(\frac{1+\sqrt{1+\epsilon^2}}{2}\right)\right)\ . \tag{A-7}$$

The phase function ψ defined in equation A-7 corresponds to the analogous term in the exact-log DMO and AMO (Liner, 1990; Zhou et al., 1996; Biondi and Vlad, 2002).

REFERENCES

Abma, R., and N. Kabir, 2006, 3D interpolation of irregular data with a POCS algorithm: Geophysics, **71**, E91–E97.

Bagaini, C., and U. Spagnolini, 1996, 2-D continuation operators and their applications: Geophysics, **61**, 1846–1858.

Biondi, B., S. Fomel, and N. Chemingui, 1998, Azimuth moveout for 3-D prestack imaging: Geophysics, **63**, 574–588.

Biondi, B., and I. Vlad, 2002, Amplitude preserving prestack imaging of irregularly sampled 3-D data: 72nd Annual International Meeting, SEG, Expanded Abstracts, 2170–2173.

Bleistein, N., and H. Jaramillo, 2000, A platform for kirchhoff data mapping in scalar models of data acquisition: Geophysical Prospecting, **48**, 135–161.

Bolondi, G., E. Loinger, and F. Rocca, 1982, Offset continuation of seismic sections: Geophysical Prospecting, **30**, 813–828.

Chauris, H., and T. Nguyen, 2008, Seismic demigration/migration in the curvelet domain: Geophysics, **73**, S35–S46.

Claerbout, J. F., 2000, Basic Earth imaging: Stanford Exploration Project, `http://sepwww.stanford.edu/sep/prof/`.

Cohen, A., I. Daubechies, and J. Feauveau, 1992, Biorthogonal bases of compactly supported wavelets: Communications on Pure and Applied Mathematics, **45**, 485–560.

Daubechies, I., and W. Sweldens, 1998, Factoring wavelet transforms into lifting steps: The Journal of Fourier Analysis and Application, **4**, 247–269.

Deregowski, S. M., and F. Rocca, 1981, Geometrical optics and wave theory of constant offset sections in layered median: Geophysical Prospecting, **29**, 374–406.

Do, M. N., and M. Vetterli, 2005, The contourlet transform: an efficient directional multiresolution image representation: IEEE Trans. Image Process., **14**, 2091–2106.

Douma, H., and M. V. de Hoop, 2007, Leading-order seismic imaging using curvelets: Geophysics, **72**, S231–S248.

Fomel, S., 2001, Three-dimensinal seismic data regularization: PhD thesis, Ph.D. thesis, Stanford University.

———, 2002, Applications of plane-wave destruction filters: Geophysics, **67**, 1946–1960.

———, 2003a, Differential azimuth moveout: 73th Annual International Meeting, SEG, Expanded Abstracts, 2068–2071a.

———, 2003b, Seismic reflection data interpolation with differential offset and shot continuation: Geophysics, **68**, 733–744.

———, 2003c, Theory of differential offset continuation: Geophysics, **68**, 718–732.

———, 2006, Towards the seislet transform: 76th Annual International Meeting, SEG, Expanded Abstracts, 2847–2851a.

Fomel, S., and Y. Liu, 2010, Seislet transform and seislet frame: Geophysics, **75**, V25–V38.

French, W. S., 1974, Two-dimensional and three-dimensional migration of model-experiment reflection profiles: Geophysics, **39**, 265–277.

Hale, D., 1991, Dip moveout processing: SEG, Course Notes Series 4.

Herrmann, F., D. Wang, G. Hennenfent, and P. Moghaddam, 2008, Curvelet-based seismic data processing: a multiscale and nonlinear approach: Geophysics, **73**, A1–A5.

Herrmann, F. J., and G. Hennenfent, 2008, Non-parametric seismic data recovery with curvelet frames: Geophysical Journal International, **173**, 233–248.

Lian, C., K. Chen, H. Chen, and L. Chen, 2001, Lifting based discrete wavelet transform architecture for JPEG2000: The 2001 IEEE International Symposium on Circuits and Systems, IEEE, II445–II448.

Liner, C., 1990, General theory and comparative anatomy of dip moveout: Geophysics, **55**, 595–607.

Liu, B., and M. D. Sacchi, 2004, Minimum weighted norm interpolation of seismic records: Geophysics, **69**, 1560–1568.

Mallat, S., 2009, A wavelet tour of signal processing, the sparse way: Academic Press, Third Edition.

Pennec, E. L., and S. Mallat, 2005, Sparse geometrical image representation with bandelets: IEEE Trans. Image Process., **14**, 423–438.

Petkovsek, M., H. S. Wilf, and D. Zeilberger, 1996, $A = B$: A K Peters Ltd.

Salvador, L., and S. Savelli, 1982, Offset continuation for seismic stacking: Geophysical Prospecting, **30**, 829–849.

Spagnolini, U., and S. Opreni, 1996, 3-D shot continuation operator: 66th Annual International Meeting, SEG, Expanded Abstracts, 439–442.

Starck, J. L., E. J. Candés, and D. L. Donoho, 2000, The curvelet transform for image denoising: IEEE Trans. Image Process., **11**, 670–684.

Sweldens, W., 1995, The lifting scheme: A new philosophy in biorthogonal wavelet constructions: Wavelet Applications in Signal and Image Processing III, Proc. SPIE 2569, 68–79.

Sweldens, W., and P. Schröder, 1996, Building your own wavelets at home, *in* Wavelets in Computer Graphics: ACM SIGGRAPH Course Notes, 15–87.

Velisavljevic, V., 2005, Directionlets: anisotropic multi-directional representation with separable filtering: PhD thesis, Ecole Polytechnique Fédérale de Lausanne.

Xu, S., Y. Zhang, D. Pham, and G. Lambaré, 2005, Antileakage Fourier transform for seismic data regularization: Geophysics, **70**, V87–V95.

Zhou, B., I. M. Mason, and S. A. Greenhalgh, 1996, An accurate formulation of log-stretch dip moveout in the frequency-wavenumber domain: Geophysics, **61**, 815–820.

Zwartjes, P., and A. Gisolf, 2007, Fourier reconstruction with sparse inversion: Geophysical Prospecting, **55**, 199–221.